Electronic Supplementary Material (ESI) for Journal of Materials Chemistry A.

Supporting Information

Bimetallic Nanoparticle Decorated Perovskite Oxide for State-of-the-art Trifunctional Electrocatalysis

Quazi Arif Islam, Rahul Majee and Sayan Bhattacharyya*

Department of Chemical Sciences and Centre for Advanced Functional Materials, Indian Institute of Science Education and Research (IISER) Kolkata, Mohanpur - 741246 India

* Email for correspondence: sayanb@iiserkol.ac.in

XRD profile of samples before and after reduction

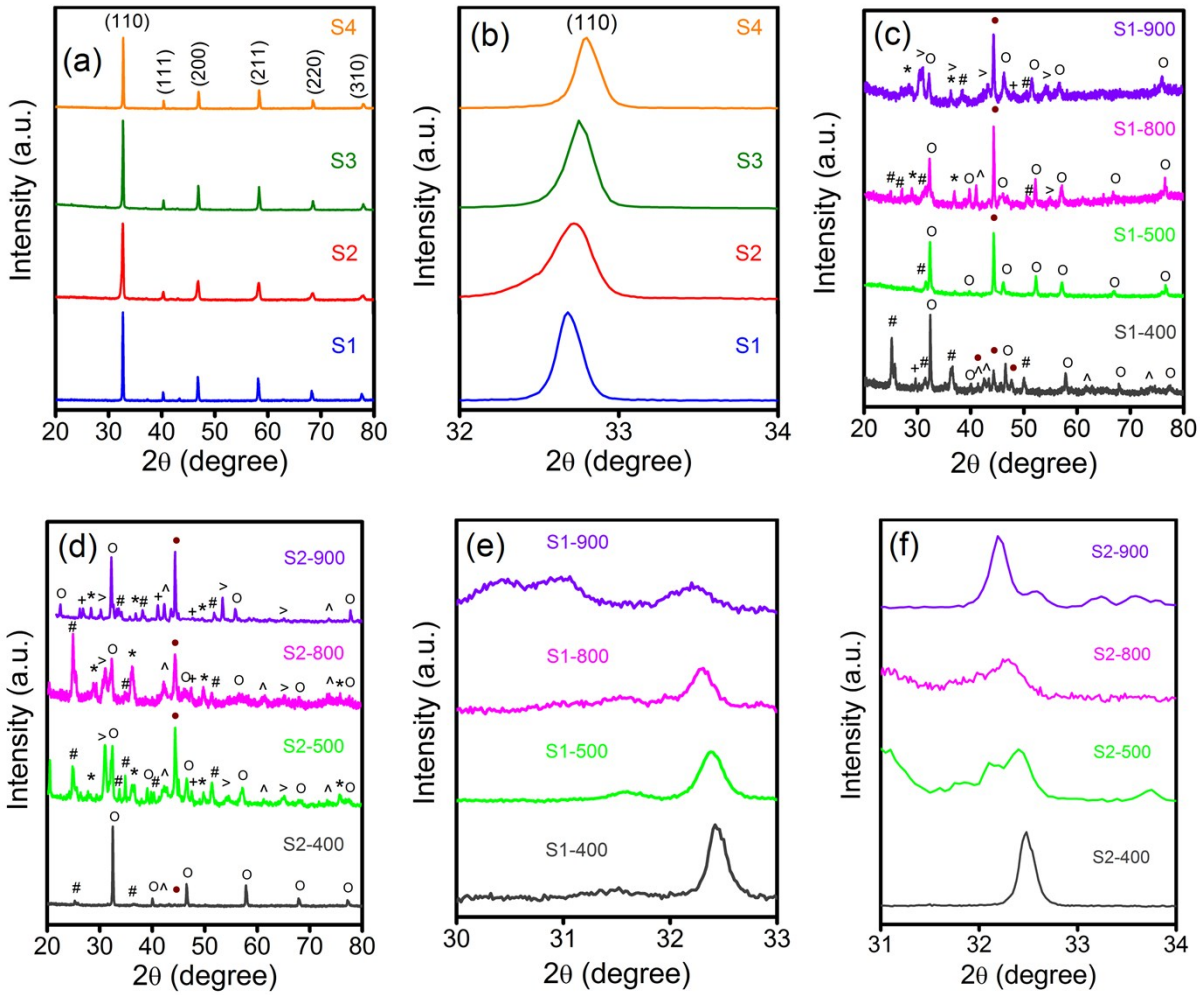

Figure S1. XRD patterns of (a) calcined powders, (b) zoomed view of (110) peak, (c) S1 reduced at different temperatures, (d) S2 reduced at different temperatures, (e) zoomed view of (110) peak of S1 reduced at different temperatures, and (f) zoomed view of (110) peak of S1 reduced at different temperatures. The symbols are: perovskite (o), NbO_2 (#), CoO (^), CoNi (●), SrO (>), Nb_2O_5 (*) and unknown phase (+).

Discussion S1. Oxygen non-stoichiometry

Oxygen nonstoichiometry of calcined SNCN and the reduced samples is calculated by thermogravimetric analysis. A known quantity of sample is reduced to individual metal oxides in H_2 atmosphere at elevated temperature. By measuring the weight change during different stages of heat treatment, the oxygen nonstoichiometry is calculated.

$m_1/M_{SNCN} = m_2/M_{SNCN\text{-}reduced}$ (1)

m_1 = mass of sample before reduction

m_2 = mass of sample after reduction

M_{SNCN} = Molecular weight of $Sr_{0.95}Co_{0.9-x}Ni_xNb_{0.1}O_{3-\delta}$ (x = 0.1 and 0.2)

$M_{SNCN\text{-}reduced}$ = Sum of molecular weights of reduced phases (SrO, CoO, NiO and Nb_2O_5)

$2Sr_{0.95}Co_{0.8}Ni_{0.1}Nb_{0.1}O_{3-\delta} + (2.2\text{-}2\delta)\ H_2 \rightarrow 1.9SrO + 1.6CoO + 0.2NiO + 0.2NbO + (2.2\text{-}2\delta)\ H_2O$ (2)

Table S1. Results of the determination of oxygen non-stoichiometry.

Sample ID	Sample weight (mg)	m_1 (mg)	m_2 (mg)	δ
S1	19.4	15.8	14.6	0.22
S2	32.2	38.8	36.3	0.28
S1-400	30.4	22.3	20.9	0.33
S2-400	42.1	23.5	22.17	0.39

Morphology of calcined samples

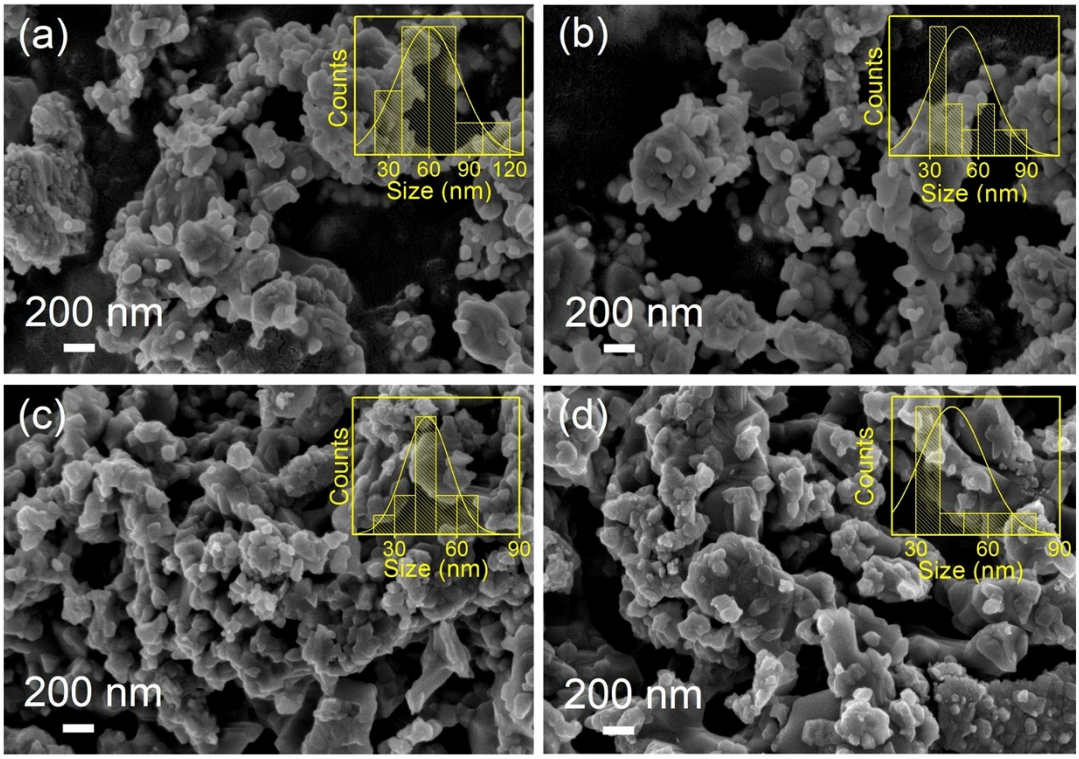

Figure S2. FESEM images of (a) S-1, (b) S-2, (c) S-3, and (d) S-4. Insets show the corresponding diameter histograms.

Morphology of S1 after reduction

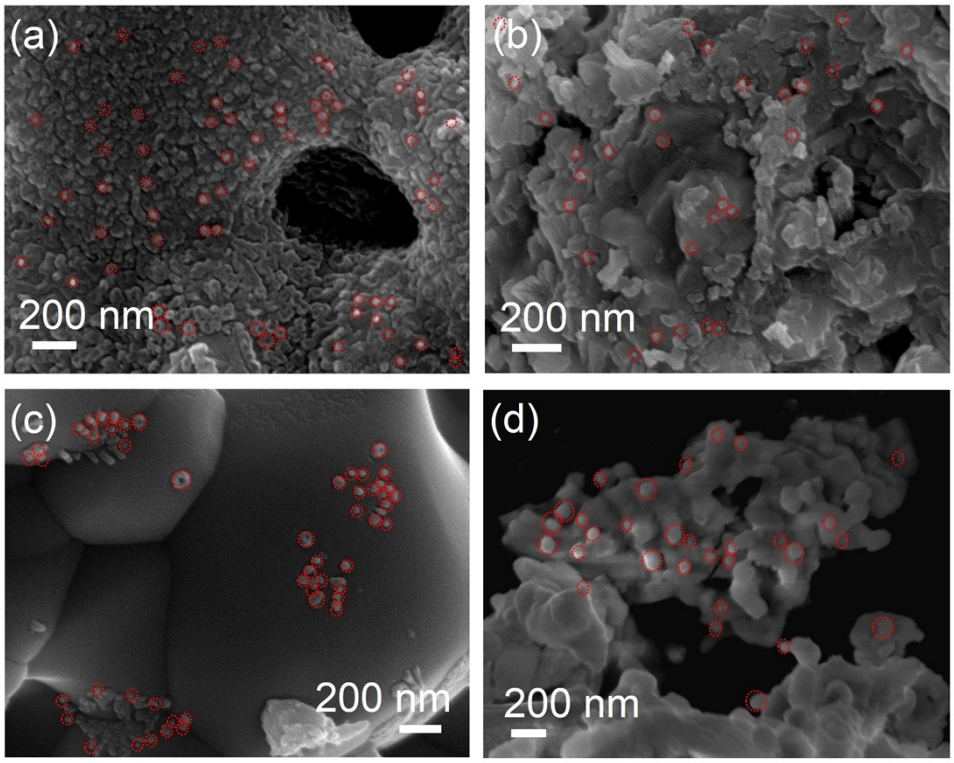

Figure S3. FESEM images of S1 after reduction at different temperatures: (a) 400°C, (b) 500°C, (c) 800°C, and (d) 900°C. Red circles indicate the exsolved NPs.

Morphology of S2 after reduction

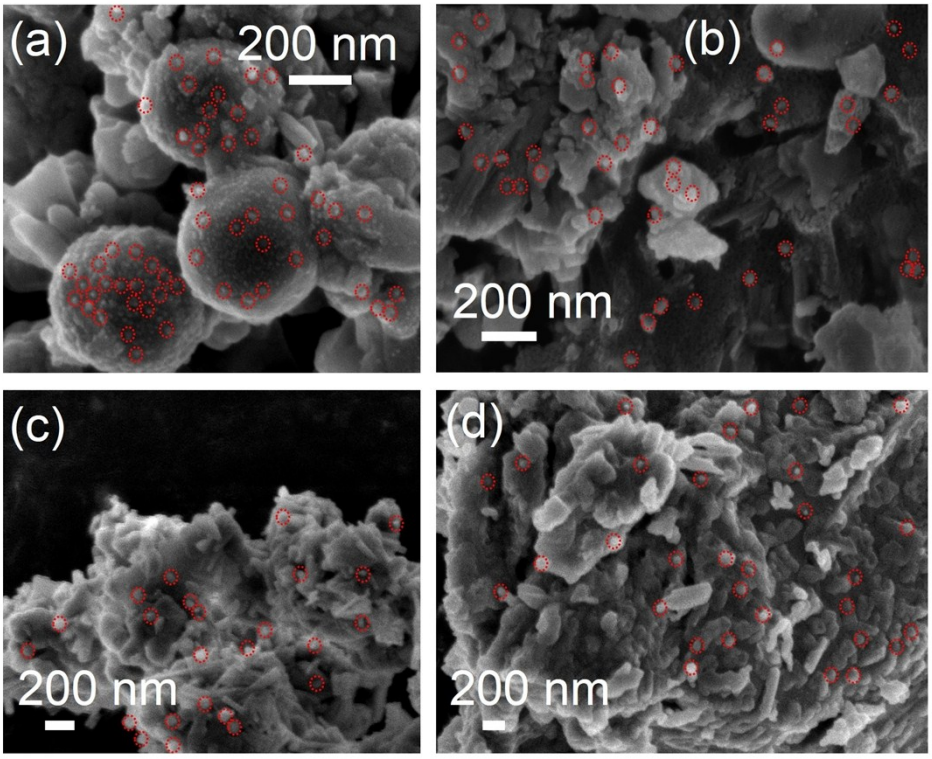

Figure S4. FESEM images of S2 after reduction at different temperatures: (a) 400°C, (b) 500°C, (c) 800°C, and (d) 900°C. Red circles indicate the exsolved NPs.

Elemental distribution of S1 and S2

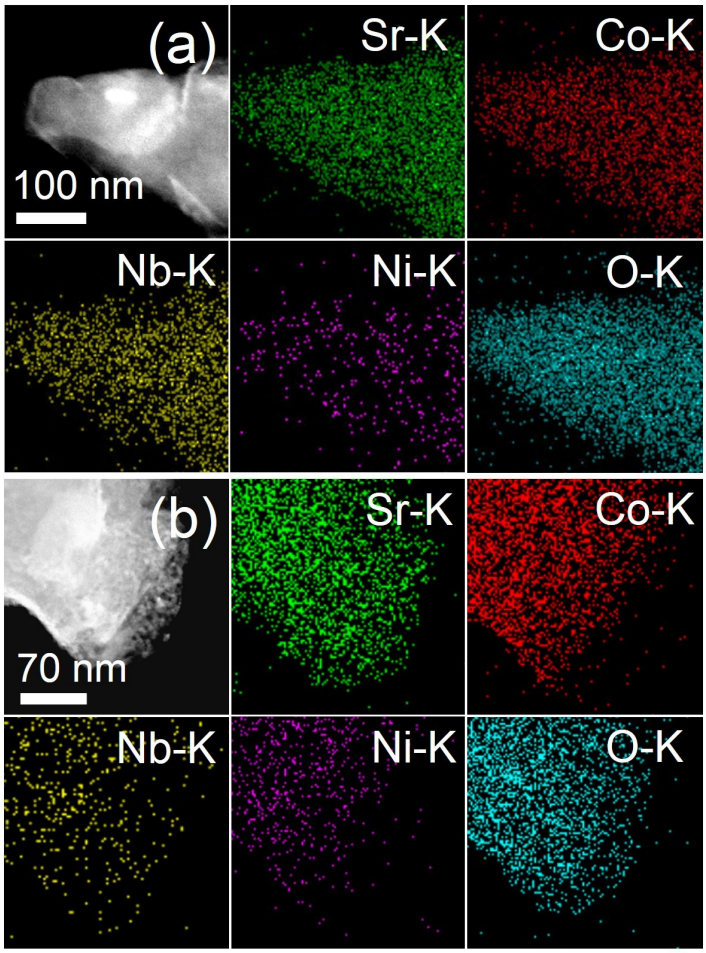

Figure S5. STEM-HAADF images and corresponding elemental maps of (a) S1 and (b) S2.

Microscopic images and elemental distribution of S1 and S2 reduced at 900°C

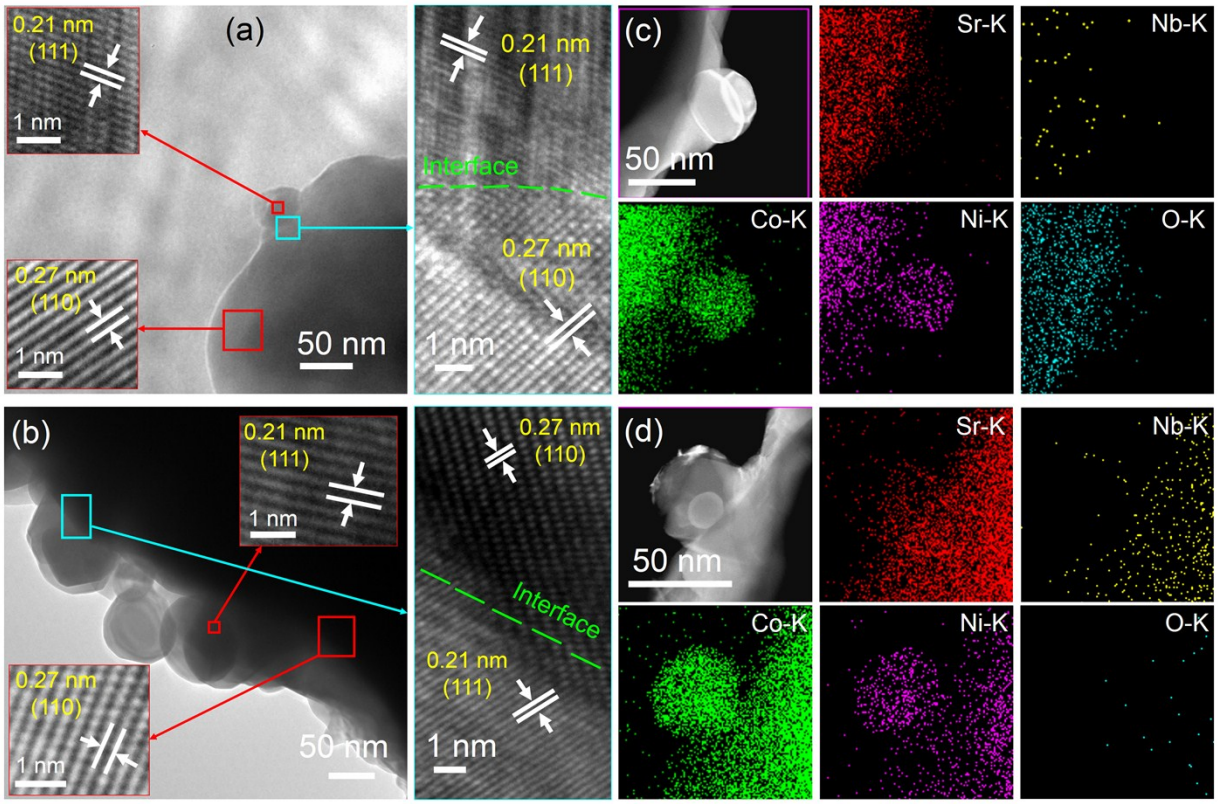

Figure S6. High resolution TEM images showing the crystallographic structure of the exsolved CoNi NPs along with the legible hetero-junction between CoNi NPs and perovskite substrate for (a) S1-900, (b) S2-900. STEM-HAADF images and elemental mapping of (c) S1-900, and (b) S2-900.

AFM images of the perovskite oxide samples after reduction at 400°C

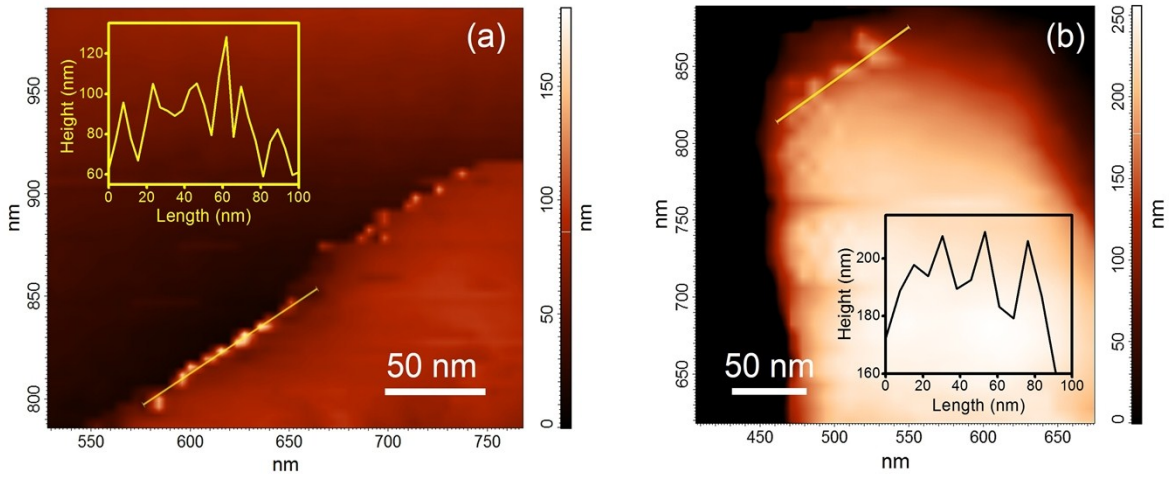

Figure S7. AFM images of (a) S1-400, and (b) S2-400. The insets show the height profile along the lines in panel (a) and (b).

XPS spectra of Sr *3d* and Nb *3d*

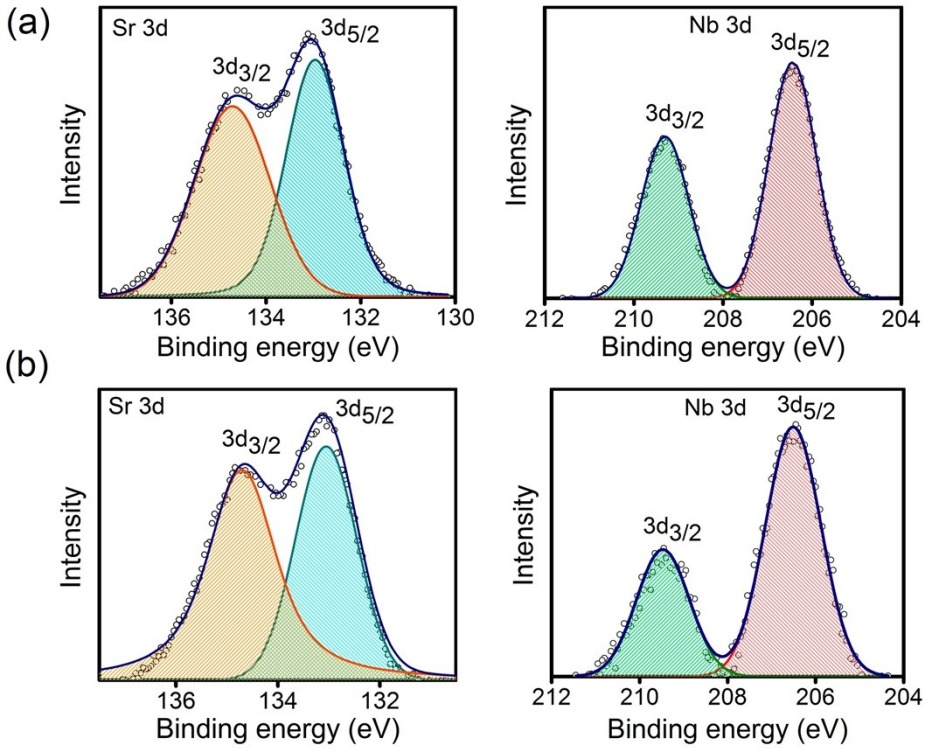

Figure S8. XPS spectra of Sr *3d* and Nb *3d* levels for (a) S1 and (b) S2.

XPS spectra of O *1s*

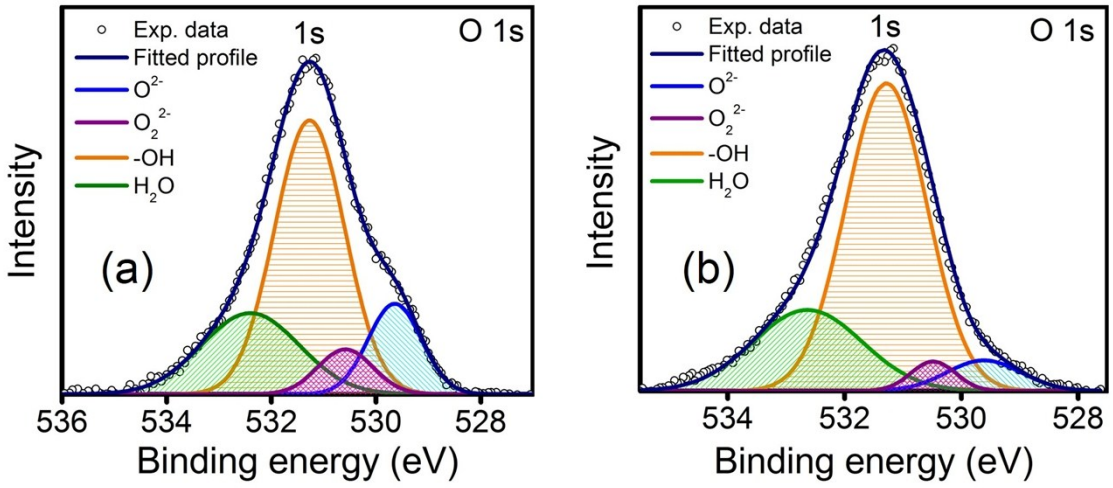

Figure S9. XPS spectra of O *1s* level for (a) S1 and (b) S2.

Table S2. Binding energies of S1 and S2.

Sample	Binding energy (eV)								
	Sr $3d_{3/2}$	Sr $3d_{5/2}$	Nb $3d_{3/2}$	Nb $3d_{5/2}$	Co $2p_{1/2}$	Co $2p_{3/2}$	Ni $2p_{1/2}$	Ni $2p_{3/2}$	O *1s*
S1	134.70	133.06	209.46	206.52	795.60	780.42	872.12	855.71	531.25
S2	134.70	132.97	209.29	206.45	795.45	780.23	872.86	855.55	531.30

Table S3. XPS peak deconvolution results of O *1s* core levels of S1 and S2.

Sample	Lattice O^{2-} (%)	O_2^{2-}/O^- (%)	-OH/O_2 (%)	H_2O (%)
S1	14.07	7.18	55.73	23.02
S2	10.50	6.06	66.05	17.39

Table S4. Tafel slopes of different perovskite oxide compositions for HER, OER and ORR.

Composition	Tafel slope (mV/dec)		
	HER	OER	ORR
$SrCoO_3$ (SC)	157	171	176
$SrCo_{0.9}Nb_{0.1}O_{3-\delta}$ (SCN)	142	153	162
$Sr_{0.95}Co_{0.8}Nb_{0.1}Ni_{0.1}O_{3-\delta}$ (S1)	64	67	90
$Sr_{0.95}Co_{0.7}Nb_{0.1}Ni_{0.2}O_{3-\delta}$ (S2)	80	96	129
$Sr_{0.95}Co_{0.6}Nb_{0.1}Ni_{0.3}O_{3-\delta}$ (S3)	101	118	128
$Sr_{0.95}Co_{0.5}Nb_{0.1}Ni_{0.4}O_{3-\delta}$ (S4)	106	145	136
Pt/C	49	-	67
IrO_2	-	71	-

Table S5. Comparison of OER and ORR electrochemical activity of S1 and S1-400 with the reported perovskite oxide catalysts.

Sl. No.	Catalyst	ORR potential [V] @ -3 mA cm^{-2} (vs. RHE)	ORR overpotential [mV] @ -3 mA cm^{-2} (vs. RHE)	OER potential [V] @ 10 mA cm^{-2} (vs. RHE)	OER overpotential [mV] @ 10 mA cm^{-2} (vs. RHE)	Reference
1.	$Sr_{0.95}Nb_{0.1}Co_{0.8}Ni_{0.1}O_{3-\delta}$	0.835	395	1.668	438	This work
2.	Reduced $Sr_{0.95}Nb_{0.1}Co_{0.8}Ni_{0.1}O_{3-\delta}$	0.883 0.937	347 (1 M KOH) 293 (0.1 M KOH)	1.614 1.659	380 (1 M KOH) 429 (0.1 M KOH)	This work
3.	Nanostructured $LaNiO_3$ nanorod/NC	0.64	590	1.66	≈430	(S1)
4.	$La_{0.95}FeO_{3-\delta}$/SP	≈0.38	850	1.61	≈410	(S2)
5.	$PrBaMn_2O_{5+\delta}$/VC	≈0.74	490	1.73	≈500	(S3)
6.	$La_{0.5}Sr_{0.5}CoO_{3-\delta}$ nanotube/KB	≈0.59	640	1.63	≈400	(S4)
7.	$Pr_{0.5}Ba_{0.5}MnCo_{0.2}O_{3-\delta}$ nanofiber/VC	≈0.70	530	1.83	≈600	(S5)
8.	$La_{0.5}Sr_{0.5}Co_{0.8}Fe_{0.2}O_3$ nanorod/NRGO	≈0.81	420	1.73	≈500	(S6)
9.	$La_{0.58}Sr_{0.4}Fe_{0.2}Co_{0.8}O_3$ nanoparticle/NCNT	≈0.58	650	1.65	≈420	(S7)
10.	$CaMn_{0.75}Nb_{0.25}O_{3-\delta}$	≈0.62	610	1.72	≈490	(S8)
11.	$La_x(Ba_{0.5}Sr_{0.5})_{1-x}Co_{0.8}Fe_{0.2}O_{3-\delta}$	0.66	570	1.65	≈420	(S9)
12.	$Ba_{0.5}Sr_{0.5}Co_{0.8}Fe_{0.2}O_{3-\delta}$	≈0.55	680	-	-	(S10)
13.	$La_{0.8}Sr_{0.2}Mn_{0.6}Ni_{0.4}O_3$ nanoparticle/VC	≈0.58	650	1.66	≈638	(S11)
14.	$LaNi_{0.85}Mg_{0.15}O_3$/VC	≈0.63	600	1.84	≈608	(S12)
15.	$LaNi_{0.8}Fe_{0.2}O_3$/VC	≈0.60	630	1.70	*≈468*	(S13)
16.	$La_{0.3}(Ba_{0.5}Sr_{0.5})_{0.7}Co0.8Fe_{0.2}O_{3-\delta}$/KB	≈0.54	690	1.54	≈315	(S14)
17.	Ball-milled $La_{0.6}Sr_{0.4}CoO_{3-\delta}$/VC	≈0.60	630	1.75	≈525	(S15)
18.	$Ba_{0.5}Sr0.5Co_{0.8}Fe_{0.2}O_{3-\delta}$/AB	≈0.66	570	1.70	≈474	(S16)
19.	$Ba_{0.9}Co_{0.5}Fe_{0.4}Nb_{0.1}O_{3-\delta}$/AB	≈0.60	630	1.66	≈434	(S17)
20.	$PrBa_{0.25}Sr_{0.75}Co_2O_{5.95}$/AB	≈0.65	580	1.65	≈420	(S18)
21.	$BaMnO_3$ nanorod/C	≈0.60	630	1.8	≈624	(S19)
22.	$Nd_{0.5}Sr_{0.5}CoO_{3-\delta}$ nanorod/IgnPs	≈0.63	600	1.65	≈425	(S20)
23.	mesoporous $Ba_{0.5}Sr_{0.5}Co_{0.8}Fe_{0.2}O_{3-\delta}$	~0.51	720		-	(S21)
24.	$NdBa_{0.5}Sr_{0.5}Co_{1.5}Fe_{0.5}O_{5+d}$	0.651	570	1.62	394	(S22)
25.	$SmBa_{0.5}Sr_{0.5}Co_{1.5}Fe_{0.5}O_{5+d}$	0.649	580	1.63	407	
26.	$GdBa_{0.5}Sr_{0.5}Co_{1.5}Fe_{0.5}O_{5+d}$	0.648	580	1.65	425	
27.	$NdBa_{0.5}Sr_{0.5}Co_{1.5}Fe_{0.5}O_{5+d}$/N-rGO	0.869	360	1.63	405	
28.	$La_{0.8}Sr_{0.2}Mn_{0.95}P_{0.05}O_{3-x}$	0.67	560		-	(S23)
29.	N-$Ca_2Fe_2O_5$	~0.35	880		-	(S24)
30.	$NdBa_{0.75}Ca_{0.25}Co_{1.5}Fe_{0.5}O_5$	~0.72	510		-	(S25)
31.	$LaMnO_3$/NC	~0.63	600		-	(S26)
32.	$LaCoO_3$/NC	0.64	590	1.64	410	
33.	$LaNi_{0.75}Fe_{0.25}O_{3-x}$/NC	~0.74	490	1.75	520	
34.	$LaTi_{0.65}Fe_{0.35}O_{3-x}$/NCNR	0.70	530		540	(S27)

FESEM image of S1 catalyst after OER stability test

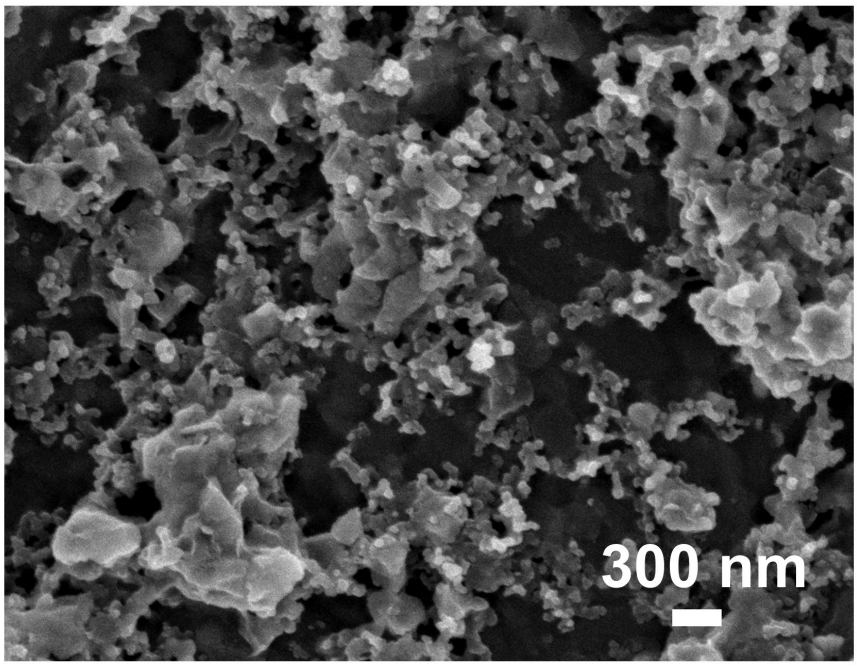

Figure S10. FESEM image of S1 after OER stability test.

ECSA, cyclic voltammograms in non-faradaic region with different scan rates and the current with scan rate plots

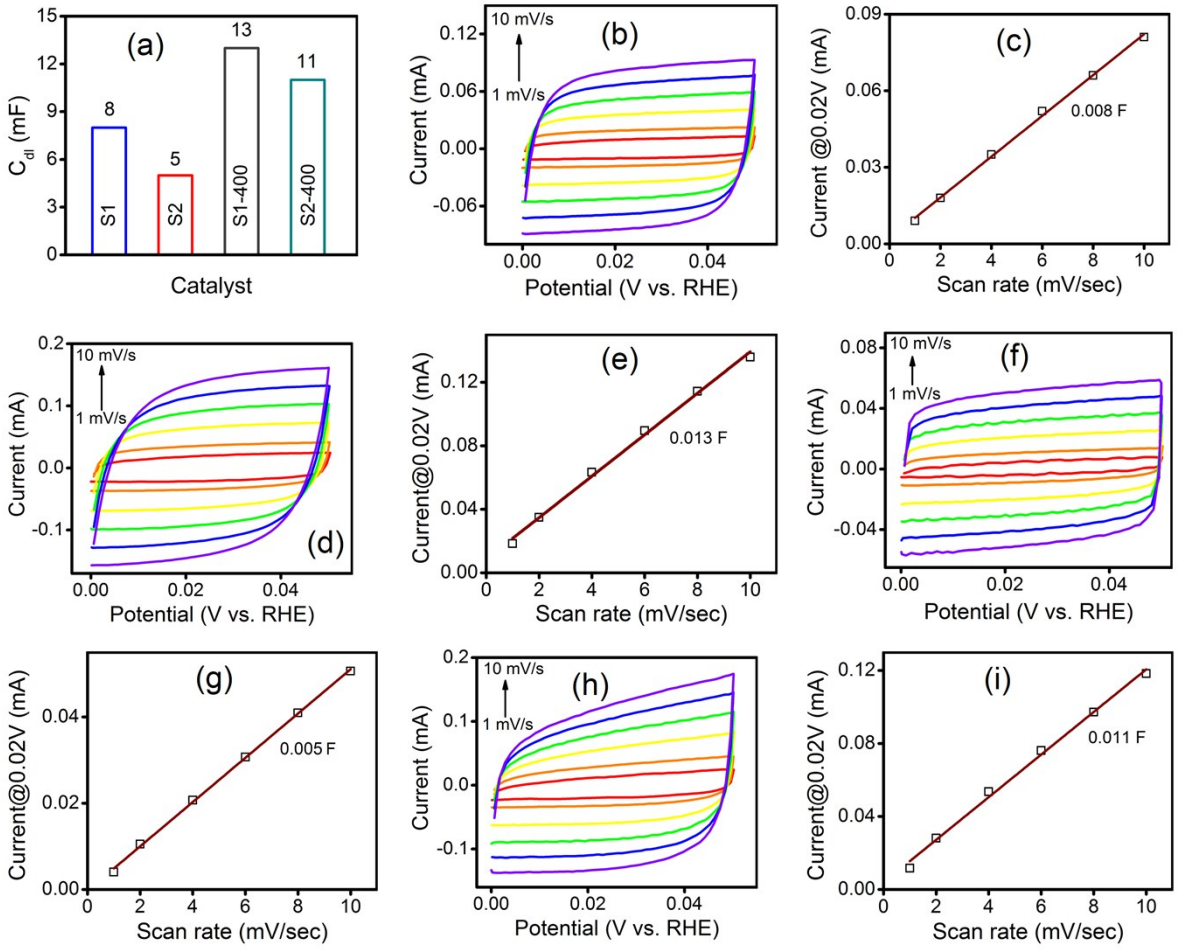

Figure S11. (a) Electrochemical double-layer capacitance (C_{dl}) values of different catalysts. Cyclic voltammograms in non-faradaic region with different scan rates and the current with scan rate plots are shown for (b-c) S1, (d-e) S1-400, (f-g) S2, and (h-i) S2-400.

Discussion S2. Calculation of turn over frequency (TOF) of S1-400 and S2-400 catalyst

Composition of the exsolved NPs (active sites) is $Co_{0.75}Ni_{0.25}$

Atomic radii of Co and Ni are 152 and 149 pm, respectively.

Surface area occupied by Ni = $4 \times 3.14 \times (149 \times 10^{-12})^2$ m^2 = 2.78×10^{-19} m^2

Surface area occupied by Co = $4 \times 3.14 \times (152 \times 10^{-12})^2$ m^2 = 2.90×10^{-19} m^2

Effective surface area of single $Co_{0.75}Ni_{0.25}$ unit = $\{(0.75 \times 2.9) + (0.25 \times 2.78)\}\ 10^{-19}$ m^2

$= 28.7 \times 10^{-20}$ m^2.

Now, since the ECSA of S1-400 is 325 cm^2.

Therefore number of $Co_{0.75}Ni_{0.25}$ units present at surface = 0.0325 m^2/ (28.7×10^{-20}) m^2

$= 1.13 \times 10^{17} = 1.88 \times 10^{-7}$ mole

Now, since the ECSA of S2-400 is 275 cm^2.

Therefore number of $Co_{0.75}Ni_{0.25}$ units present at surface = 0.0275 m^2/ (28.7×10^{-20}) m^2

$= 9.58 \times 10^{16} = 1.59 \times 10^{-7}$ mole

Now, for HER, TOF = $\frac{1}{2}$.(I/F.n), where, I is the current (in A) during LSV measurement, F is Faraday constant (in C mol^{-1}) and N is number of active sites (in mol).

The factor $\frac{1}{2}$ in the equation above represents the requirement of two electrons to form one hydrogen molecule from two protons ($2H^+ + 2e = H_2$).

In case of OER, TOF = $\frac{1}{4}$.(I/F.n)

The factor $\frac{1}{4}$ in this equation represents the participation of four electrons to form one oxygen molecule ($2H_2O = H_2 + 4H^+ + 4e$).

So, TOF for S1-400 for HER = $0.006/(0.5 \times 96500 \times 1.88 \times 10^{-7}) = 0.66$ s^{-1} at overpotential of 300 mV versus RHE.

So, TOF for S2-400 for HER = $0.016/(0.5 \times 96500 \times 1.59 \times 10^{-7}) = 2.08$ s^{-1} at overpotential of 300 mV versus RHE.

The TOF for S1-400 for OER = $0.0005/(0.25 \times 96500 \times 1.88 \times 10^{-7}) = 0.11$ s^{-1} at overpotential of 300 mV versus RHE.

The TOF for S2-400 for OER = $0.0001/(0.25 \times 96500 \times 1.59 \times 10^{-7}) = 0.03$ s^{-1} at overpotential of 300 mV versus RHE.

Comparison of ORR onset potential

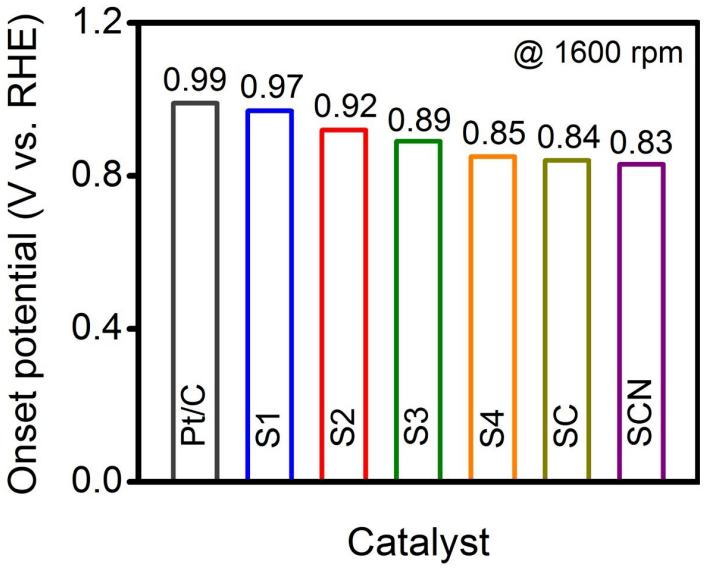

Figure S12. ORR onset potential with the catalysts of different compositions.

Cyclic voltammograms of S1 at different conditions

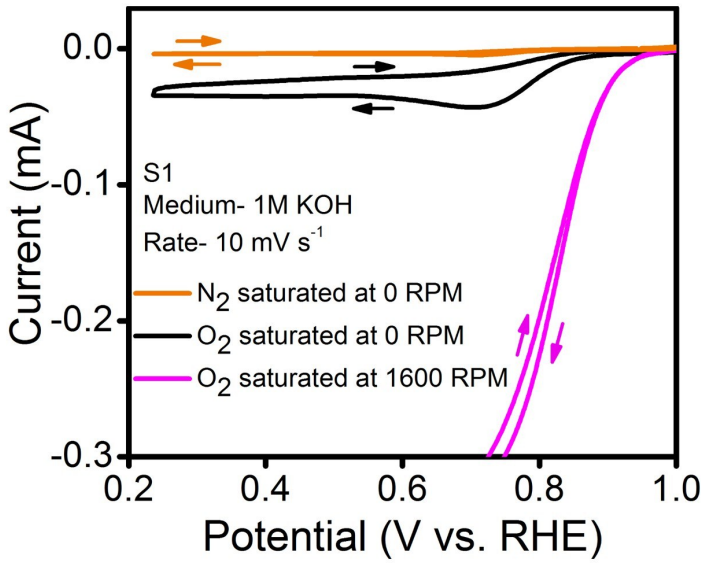

Figure S13. Cyclic voltammograms of S1 at 10 mV s^{-1} in 1 M KOH at room temperature in N_2-saturated electrolyte at 0 rpm (orange) or in O_2-saturated electrolyte at 0 rpm (black) and 1600 rpm (pink). Sweep directions are shown by the arrow.

FESEM image of the catalyst after ORR stability test

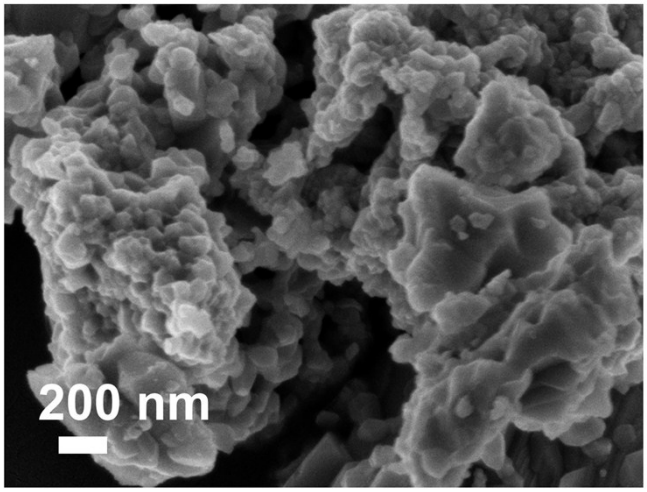

Figure S14. FESEM image of S1 after ORR stability test.

Table S6. Comparison of HER electrochemical activity of S2 and S2-400 with the reported catalysts.

Sl. No.	Composition	Electrolyte	Tafel Slope (mV dec^{-1})	HER overpotential [mV] @ -10 mA cm^{-2}	Substrate	Reference
1.	$Sr_{0.95}Nb_{0.1}Co_{0.7}Ni_{0.2}O_{3-\delta}$	1.0 M KOH	64	299	Carbon paper	This work
2.	Reduced $Sr_{0.95}Nb_{0.1}Co_{0.7}Ni_{0.2}O_{3-\delta}$		-	208 (pH 14) 183 (pH 0)		
		0.1 M KOH	-	274 (pH 13)		
3.	$Ba_{0.5}Sr_{0.5}Co_{0.8}Fe_{0.2}O_{3-\delta}$	1.0 M KOH	75±1	342±2	Glassy carbon (GC)	(S28)
4.	$Pr_{0.5}(Ba_{0.5}Sr_{0.5})_{0.5}Co_{0.8}Fe_{0.2}O_{3-\delta}$	1.0 M KOH	45±1	237±2	GC	
5.	$SrNb_{0.1}Co_{0.7}Fe_{0.2}O_{3-\delta}$ nanorods	0.1 M KOH	134	262	GC	(S29)
		1.0 M KOH	103	232		
6.	Layered $NdBaMn_2O_{5.5}$	1.0 M KOH	87	290	Ni foam	(S30)
7.	CoP/CC		129	209	Carbon cloth	(S31)
8.	PNC/Co	1.0 M KOH	76	298	GC	(S32)
9.	Co_3O_4 NCs/CFP	1.0 M KOH	116	380	C fiber	(S33)
10.	MoB	1.0 M KOH	59	220	-	(S34)

11.	Mn_1N_1	0.1 M KOH	NA	360	GC	(S35)
12.	$Ni_{2/3}Fe_{1/3}$-rGO	1.0 M KOH	210	550	GC	(S36)
13.	Co-NRCNTs	1.0 M KOH	NA	370	GC	(S37)
14.	$Co_{0.6}Mo_{1.4}N_2$	0.1 M KOH	-	280	GC	(S38)

FESEM image of the catalyst after HER stability test

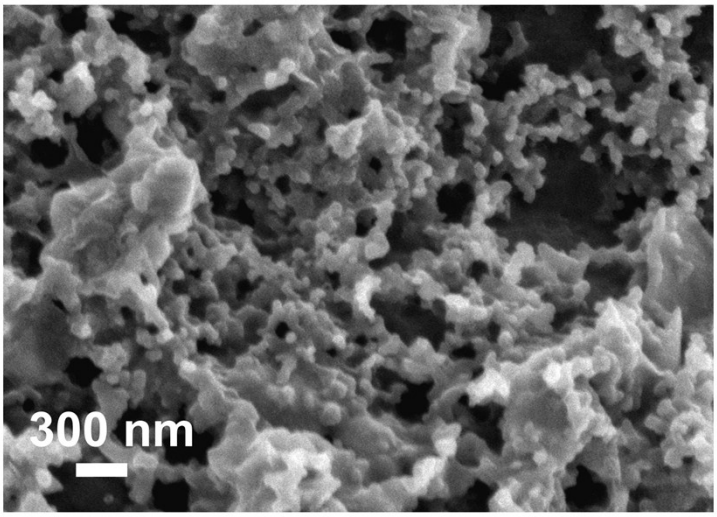

Figure S15. FESEM image of S2 after HER stability test.

Structural stability catalysts after stability test

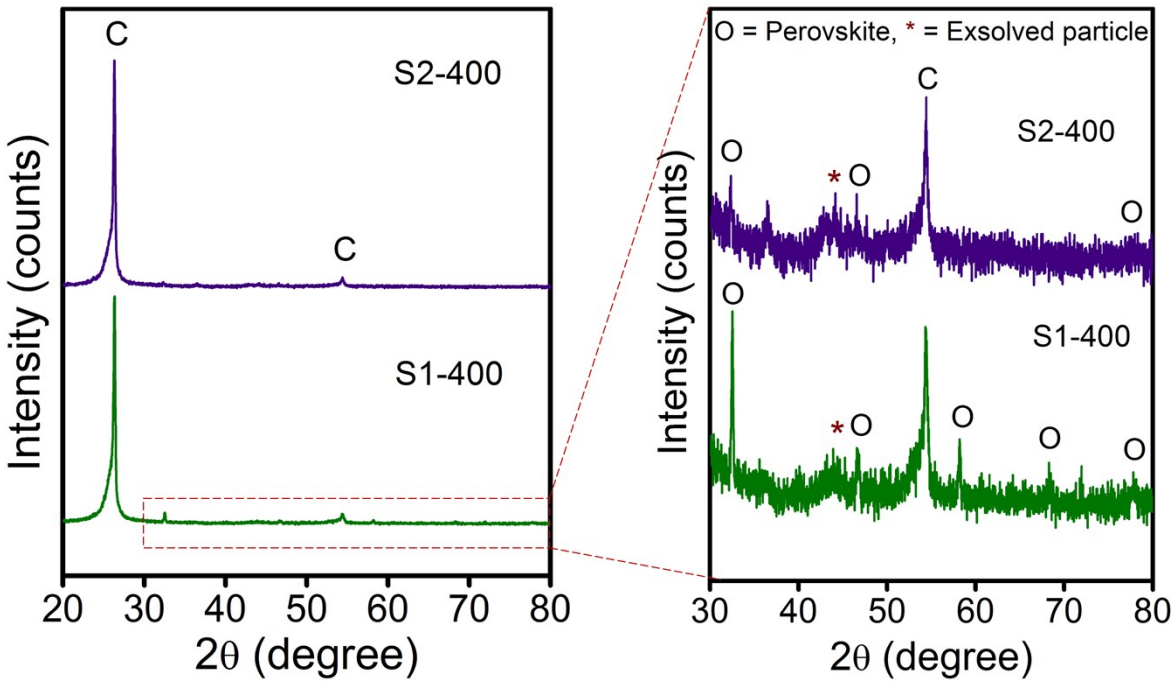

Figure S16. X-ray diffractograms of S1-400 and S2-400 working electrode after OER and HER stability tests.

pH universal HER activity of S2-400

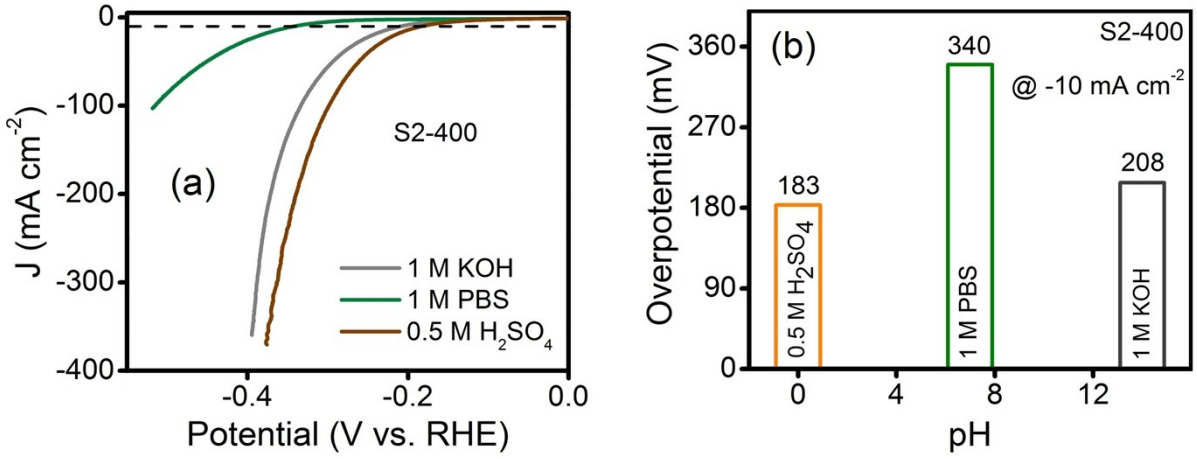

Figure S17. (a) HER polarization curves of S2-400 at different pH (with different electrolytes). (b) The overpotential required to achieve -10 mA cm^{-2}.

Overall water splitting

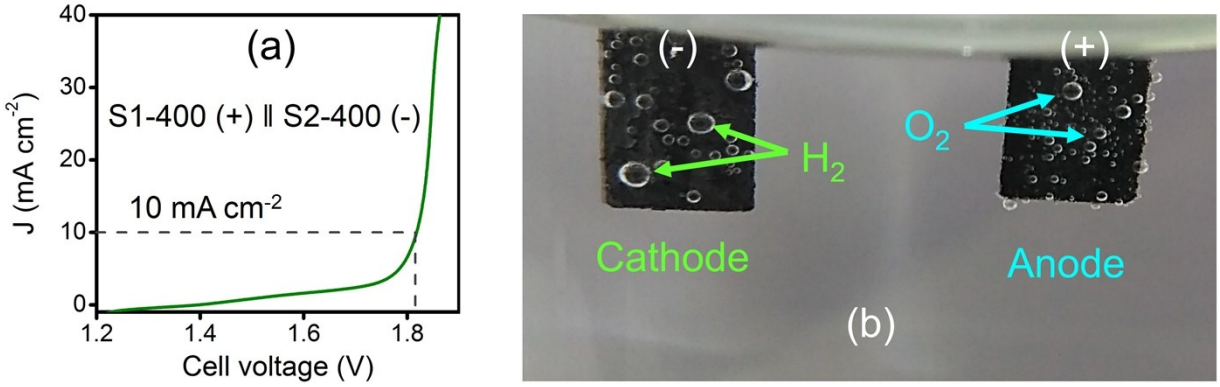

Figure S18. (a) Polarization curves of the two-electrode setup with bifunctional catalysts for overall water-splitting in 1 M KOH. (b) The optical image of O_2 and H_2 bubble generation during water splitting at a cell voltage of 1.81 V.

HER and OER of S1-400 in different media

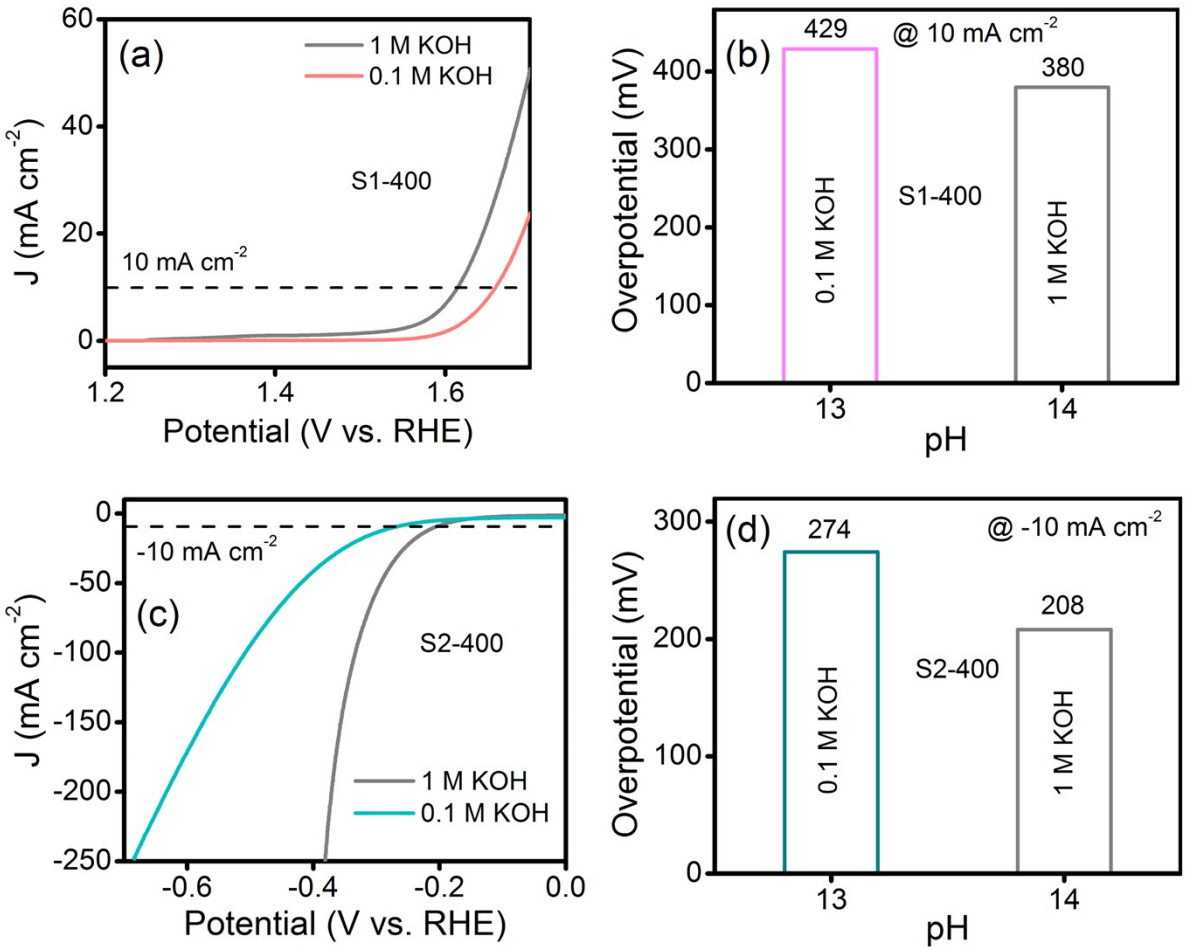

Figure S19. (a) OER polarization curves for S1-400 in 1.0 and 0.1 M KOH, (b) corresponding bar plot of overpotentials to achieve 10 mA cm^{-2}, (c) HER polarization curves for S1-400 in 1.0 and 0.1 M KOH, and (d) corresponding bar plot of overpotentials to achieve -10 mA cm^{-2}.

RDE and RRDE measurements

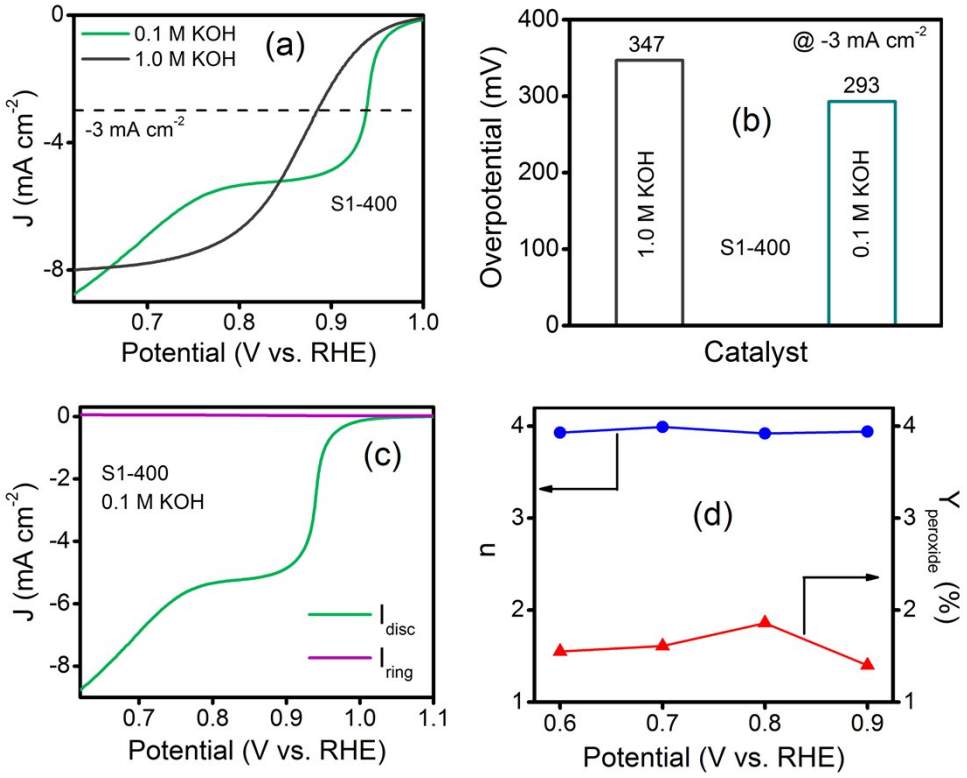

Figure S20. (a) LSV curves of S1-400 at a rotating rate of 1600 rpm in oxygen saturated 1.0 M and 0.1 M KOH, (b) required overpotentials to achieve -3 mA cm^{-2}, (c) ORR disk (I_{disc}) and ring currents (I_{ring}) collected during RRDE experiment of S1-400 electrode in O_2-saturated 0.1 M KOH, and (d) Calculated electron-transfer number *n* and H_2O_2 yield from RRDE data.

Mechanism of electrocatalytic processes

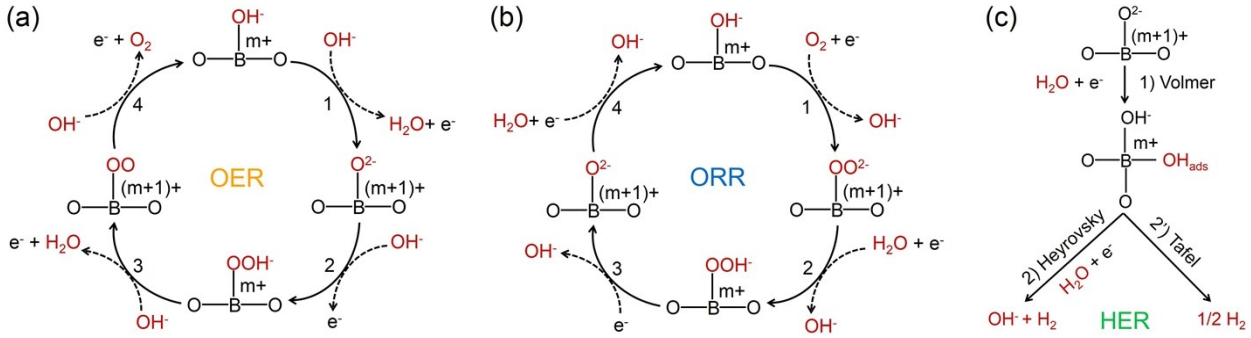

Figure S21. Proposed mechanisms on perovskite oxide catalyst in alkaline medium (a) OER, (b) ORR, and (c) HER.

OER, ORR of S1-400 and HER of S2-400 with/without carbon black

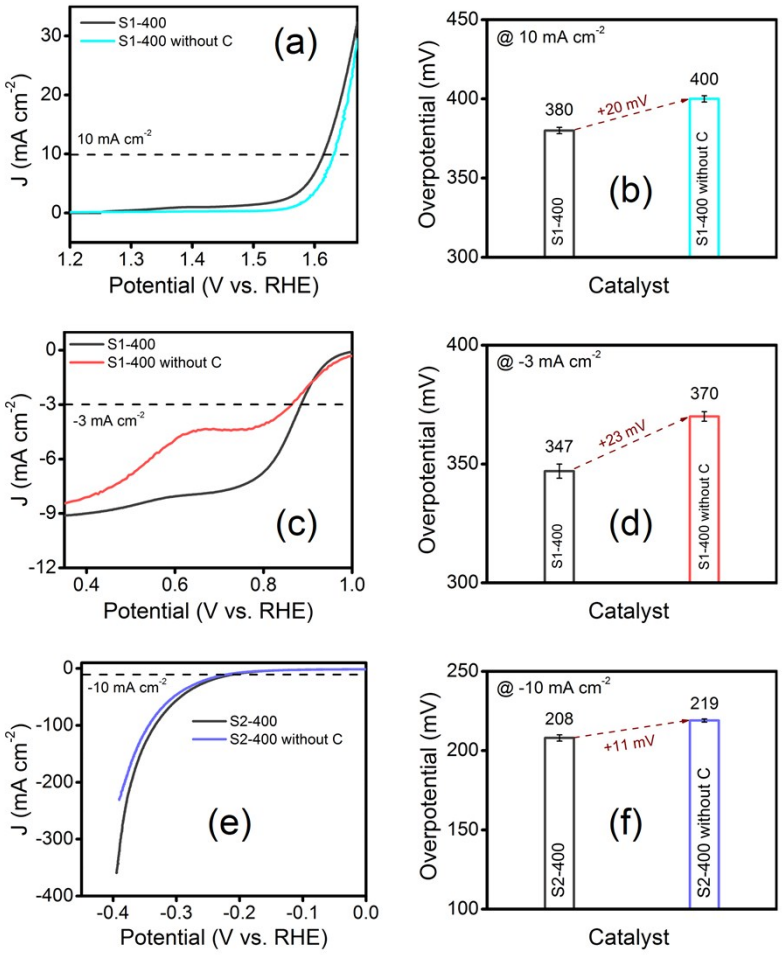

Figure S22. Evaluation of trifunctional activities with and without 10 wt% carbon black in 1 M KOH. Panels on the left show the LSV polarization plots and right panels show the overpotential bar plots. (a, b) OER activity of S1-400 measured at 10 mA cm^{-2}, (c, d) ORR activity of S1-400 measured at -3 mA cm^{-2}, (e-f) HER activity of S2-400 measured at -10 mA cm^{-2}.

Effect of scavenger addition at different potentials

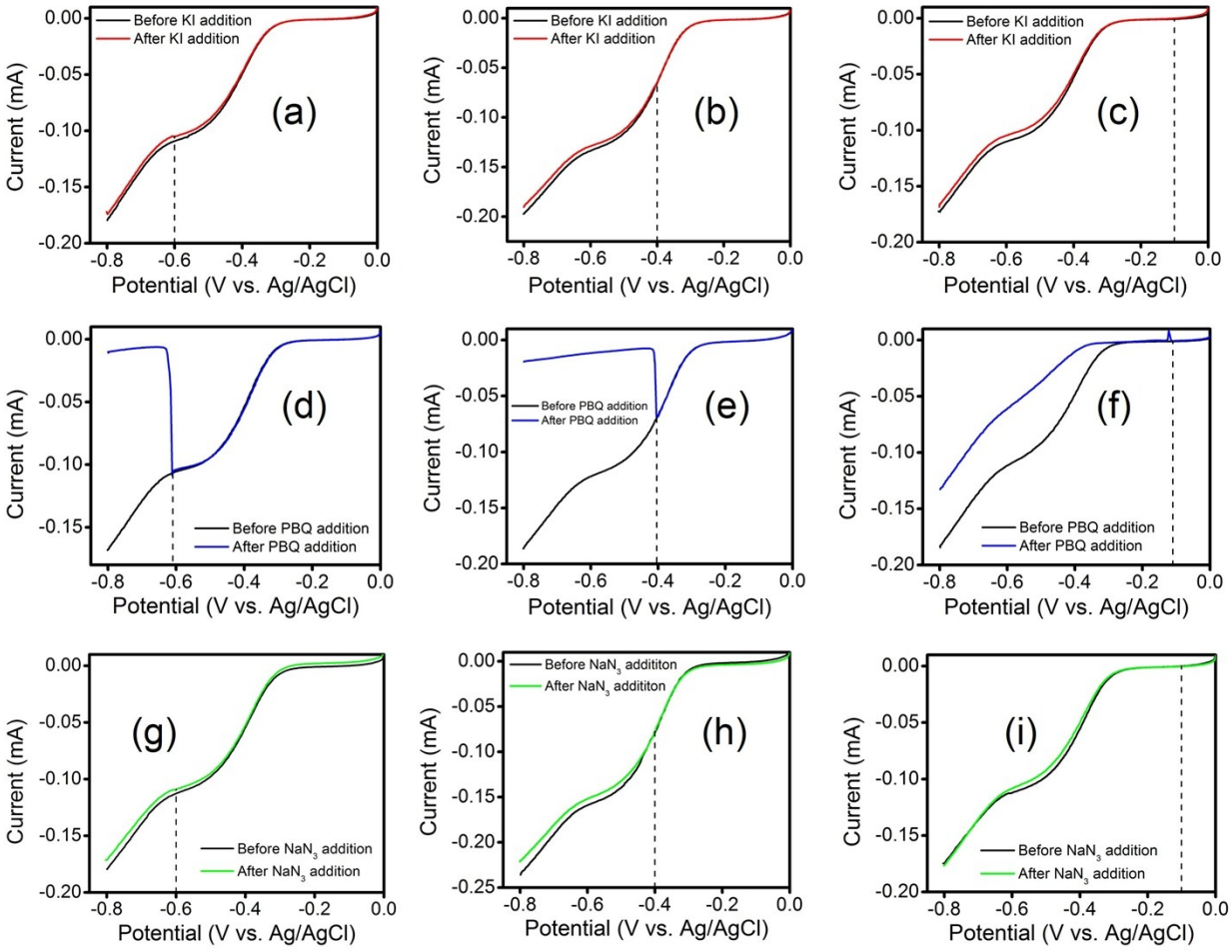

Figure S23. Effect of the addition of scavengers (a-c) KI, (d-f) p-benzoquinone and (g-i) NaN_3 at different potentials, -0.6, -0.4 and -0.1 V (L-R), during LSV test for ORR.

References

S1 W. G. Hardin, D. A. Slanac, X. Wang, S. Dai, K. P. Johnston and K. J. Stevenson, *J. Phys. Chem. Lett.*, 2013, **4**, 1254-1259.

S2 Y. Zhu, W. Zhou, J. Yu, Y. Chen, M. Liu and Z. Shao, *Chem. Mater.*, 2016, **28***,* 1691-1696.

S3 D. Chen, J. Wang, Z. Zhang, Z. Shao and F. Ciucci, *Chem. Commun.*, 2016, **52**, 10739-10742.

S4 G. Liu, H. Chen, L. Xia, S. Wang, L. X. Ding, D. Li, K. Xiao, S. Dai and H. Wang, *ACS Appl. Mater. Interfaces*, 2015, **7**, 22478-22486.

S5 Y. Zhang, Y. F. Sun and J. L. Luo, *ECS Trans.*, 2016, **75**, 955-964.

S6 H. W. Park, D. U. Lee, P. Zamani, M. H. Seo, L. F Nazar and Z. Chen, *Nano Energy*, 2014, **10**, 192-200.

S7 K. Elumeeva, J. Masa, J. Sierau, F. Tietz, M. Muhler and W. Schuhmann, *Electrochim. Acta*, 2016, **208**, 25-32.

S8 Y. Q. Lyu and F. Ciucci, *ACS Appl. Mater. Interfaces*, 2017, **9**, 35829-35836.

S9 J. -I. Jung, M. Risch, S. Park, M. G. Kim, G. Nam, H. Y. Jeong, Y. S. Horn and J. Cho, *Energy Environ. Sci.*, 2016, **9**, 176-183.

S10 J. -I. Jung, S. Park, M. G. Kim and J. Cho, *Adv. Energy Mater.*, 2015, **5**, 1501560.

S11 Z. Wang, Y. You, J. Yuan, Y. X. Yin, Y. T. Li, S. Xin and D. Zhang, *ACS Appl. Mater. Interfaces*, 2016, **8**, 6520-6528.

S12 Z. Du, P. Yang, L. Wang, Y. Lu, J.B. Goodenough, J. Zhang and D. Zhang, *J. Power Sources*, 2014, **265**, 91-96.

S13 D. Zhang, Y. Song, Z. Du, L. Wang, Y. Li and J. B. Goodenough, *J. Mater. Chem. A*, 2015, **3**, 9421-9426.

S14 J. -I. Jung, H. Y. Jeong, J. S. Lee, M. G. Kim and J. Cho, *Angew. Chem. Int. Ed.*, 2014, **53**, 4582-4588.

S15 M. Y. Oh, J. S. Jeon, J. J. Lee, P. Kim and K. S. Nahm, *RSC Adv.*, 2015, **5**, 19190-19198.

S16 C. Jin, X. Cao, F. Lu, Z. Yang and R. Yang, *Int. J. Hydrogen. Energy*, 2013, **38**, 10389-10393.

S17 C. Jin, Z. Yang, X. Cao, F. Lu and R. Yang, *Int. J. Hydrogen. Energy*, 2014, **39**, 2526-2530.

S18 Z. Wu, L. P. Sun, T. Xia, L. H. Huo, H. Zhao, A. Rougier and J. C. Grenier, *J. Power Sources*, 2016, **334**, 86-93.

S19 Y. Xu, A. Tsou, Y. Fu, J. Wang, J. H. Tian and R. Yang, *Electrochim. Acta*, 2015, **174**, 551-556.

S20 C. Kim, O. Gwon, I. Y. Jeon, Y. Kim, J. Shin, Y. W. Ju, J. B. Baek and G. Kim, *J. Mater. Chem. A*, 2016, **4**, 2122-2127.

S21 X. Cui, R. O'Hayre, S. Pylypenko, L. Zhang, L. Zeng, X. Zhang, Z. Hua, H. Chen and J. Shi, *Dalton Trans.*, 2017, **46**, 13903-13911.

S22 N. I. Kim, R. A. Afzal, S. R. Choi, S. W. Lee, D. Ahn, S. Bhattacharjee, S. C. Lee, J. H. Kim and J. Y. Park, *J. Mater. Chem. A*, 2017, **5**, 13019-13031.

S23 Y. Shen, Y. Zhu, J. Sunarso, D. Guan, B. Liu, H. Liu, W. Zhou and Z. Shao, *Chem. Eur. J.*, 2018, **24**, 6950.

S24 C. P. Jijil, M. Lokanathan, S. Chithiravel, C. Nayak, D. Bhattacharyya, S. N. Jha, P. D. Babu, B. Kakade and R. N. Devi, *ACS Appl. Mater. Interfaces.*, 2016, **8**, 34387-34395.

S25 B. Hua, Y. Q. Zhang, N. Yan, M. Li, M. Sun, Y. F. Sun, J. Chen, J. Li and J. L. Luo, *Adv. Funct. Mater.*, 2016, **26**, 4106-4112.

S26 W. G. Hardin, J. T. Mefford, D. A. Slanac, B. B. Patel, X. Wang, S. Dai, X. Zhao, R. S. Ruoff, K. P. Johnston and K. J. Stevenson, *Chem. Mater.*, 2014, **26**, 3368-3376.

S27 M. Prabu, P. Ramakrishnan, P. Ganesan, A. Manthiram and S. Shanmugam, *Nano Energy*, 2015, **15**, 92-103.

S28 X. Xu , Y. Chen , W. Zhou , Z. Zhu , C. Su , M. Liu and Z. Shao, *Adv. Mater.*, 2016, **28**, 6442-6448.

S29 Y. Zhu, W. Zhou, Y. Zhong, Y. Bu, X. Chen, Q. Zhong, M. Liu and Z. Shao, *Adv. Energy Mater.*, 2017, **7**, 1602122.

S30 J. Wang, Y. Gao, D. Chen, J. Liu, Z. Zhang, Z. Shao and F. Ciucci, *ACS Catal.*, 2018, **8**, 364-371.

S31 J. Tian, Q. Liu, A. M. Asiri and X. Sun, *J. Am. Chem. Soc.*, 2014, **136**, 7587-7590.

S32 X. Li, Z. Niu, J. Jiang and L. Ai, *J. Mater. Chem. A*, 2016, **4**, 3204-3209.

S33 S. Du, Z. Ren, J. Zhang, J. Wu, W. Xi, J. Zhu and H. Fu, *Chem. Commun.*, 2015, **51**, 8066-8069.

S34 H. Vrubel and X. Hu, *Angew. Chem., Int. Ed.,* 2012, **51**, 12703-12706.

S35 M. Ledendecker, G. Clavel, M. Antonietti and M. Shalom, *Adv. Funct. Mater.*, 2015, **25**, 393-399.

S36 W. Ma, R. Ma, C. Wang, J. Liang, X. Liu, K. Zhou and T. Sasaki, *ACS Nano*, 2015, **9**, 1977-1984.

S37 X. Zou, X. Huang, A. Goswami, R. Silva, B. R. Sathe, E. Mikmekova and T. Asefa, *Angew. Chem. Int. Ed.*, 2014, **53**, 4372-4376.

S38 B. Cao, G. M. Veith, J. C. Neuefeind, R. R. Adzic and P. G. Khalifah, *J. Am. Chem. Soc.*, 2013, **135**, 19186-19192.